DOI: 10.1002/anie.201003316

Drug Delivery

Nanoparticle-Mediated Delivery of Bleomycin**

Thomas Georgelin, Sophie Bombard, Jean-Michel Siaugue, and Valérie Cabuil*

The occurrence of side effects induced by poor distribution of antitumor agents is still an important problem in cancer treatment.[1] The challenge consists of both improving the tumor bioavailability of drugs and confining them as closely as possible to their biological targets.[2] The use of nanoparticles as vectors for drug delivery has been intensively documented during the last two decades.[3] Some of them (iron- and gold-based nanoparticles, quantum dots) are at the same time agents for imaging, thus allowing the simultaneous follow-up of the treatment efficiency.[4] They can also take part in the treatment: magnetic nanoparticles can be used for hyperthermia,[5] while gold-based nanoparticles can be used for photothermal therapy.[6]

The use of nanometric vectors brings some answers to the problem of bioavailability. Considering their large surface-to-volume ratio, they offer the possibility of transporting major quantities of drugs. Thanks to passive and active targeting, they ensure limited harmful systemic distribution. Indeed, taking into account the enhanced permeation and retention (EPR) effects, suitable nanoparticles can carry drugs into solid tumors.[7] Moreover, the grafting of targeting moieties, such as antibodies or folic acid, onto the particles' surface allows active targeting, thus decreasing the interaction with healthy cells.[8]

The efficiency of treatments is also limited because of intracellular drug resistance mechanisms: only a small amount of an agent reaches its biological target.[9] Significant improvement in drug efficiency could be obtained through the development of therapeutic strategies to pass drugs across the biological barriers. From this point of view, nanoparticles appear to be good candidates for drug delivery, because they are internalized in cells mainly by endocytosis pathways.[10] Nevertheless, nanoparticles suffer from two major limitations: the alteration of their surface in biological media and their in vivo stealth.[11] To cope with these two main problems, hybrid systems have been designed, which combine inorganic cores with organic or inorganic shells.[12] Therapeutic molecules can either be inserted into the shell or grafted onto it. One should also mention the association with polymers such as polyethylene glycol that are able to ensure both stealth and in vivo stability.[13]

The strategy we propose herein is based on the use of multifunctional core–shell nanoparticles made of γ-Fe_2O_3@SiO_2-PEG-NH_2 (PEG = polyethylene glycol), which allow covalent anchoring of biomolecules.[14] Compared with a nanometric system incorporating drugs, the grafting of an antineoplastic agent at the surface allows a drastic reduction in the uncontrolled release of the agent and thus in side effects in healthy tissues. We have chosen in this work to study the grafting of bleomycin-A5 (BLM-A5), an anticancer drug that chelates metals such as Fe^{II} and catalyzes the formation of single-stranded (ss) or double-stranded (ds) DNA lesions in the presence of oxygen.[15] The therapeutic efficiency of bleomycin (BLM) is severely limited because of its side effects, notably strong pulmonary toxicity. Dispensing the drug at lower doses near the biological target could lead to its wider use in oncology. Moreover, the delivery of this drug has been poorly studied, mainly using micrometric systems, such as glass beads[16] or polyvinylpyridine microgels.[17]

The nanoplatforms we propose are core–shell magnetic nanoparticles (CSMNs) obtained using a procedure developed by our group (Figure 1 A).[14] The core consists of citrate-coated maghemite nanoparticles (γ-Fe_2O_3, diameter around 7 nm).[18,19] The shell is a layer of silica, twice functionalized by PEG chains, to hide the nanoparticles from the reticuloendothelial system (RES),[13] and by amino groups to ensure BLM-A5 anchoring. Following van Blaaderen's method, fluorescent CSMNs can be synthesized by addition of rhodamine isothiocyanate-derived 3-aminopropyltriethoxysilane (APTS) during the coating of the magnetic cores by silica.[20] These core–shell particles are characterized by a mean hydrodynamic diameter of 40 nm, and transmission electron microscopy (TEM) images display spherical particles with a mean physical diameter of 35 nm (Figure 1 B). These particles are positively charged (+14 mV), and the surface density of amino groups can be tuned by varying the APTS to 2-[methoxy(polyethyleneoxy)propyl]trimethoxysilane (PEOS) ratio. Such particles, with different surface densities of amino groups, have been reported previously and have been fully characterized using capillary zone electrophoresis.[21]

The magnetic properties of the maghemite cores, which contain from two to three γ-Fe_2O_3 nanoparticles, are not modified by encapsulation. These CSMNs can be dispersed in 150 mM 3-(*N*-morpholino)propanesulfonic acid (MOPS) buffer at pH 7.4 or in other media with high concentrations of salts and/or proteins, while maintaining colloidal stability at room temperature for at least six months. BLM-A5 (Figure 1 C) was covalently anchored onto these platforms

[*] T. Georgelin, Dr. J.-M. Siaugue, Prof. V. Cabuil
Physicochimie des Electrolytes, Colloïdes et Sciences Analytiques (PECSA), UMR 7195 UPMC-CNRS-ESPCI-ENSCP
Université Pierre et Marie Curie Univ Paris 06, CC 51
4 place Jussieu, 75252 Paris Cedex 05 (France)
Fax: (+33) 1-4427-3228
E-mail: jean-michel.siaugue@upmc.fr
Homepage: http://www.pecsa.upmc.fr
Dr. S. Bombard
UMR 8601/UMR-S INSERM 1007, Université Paris Descartes
45 rue des Saint-Pères, 75006 Paris Cedex 06 (France)

[**] The authors would like to thank Aude Michel and Delphine Talbot for technical assistance.

Supporting information for this article is available on the WWW under http://dx.doi.org/10.1002/anie.201003316.

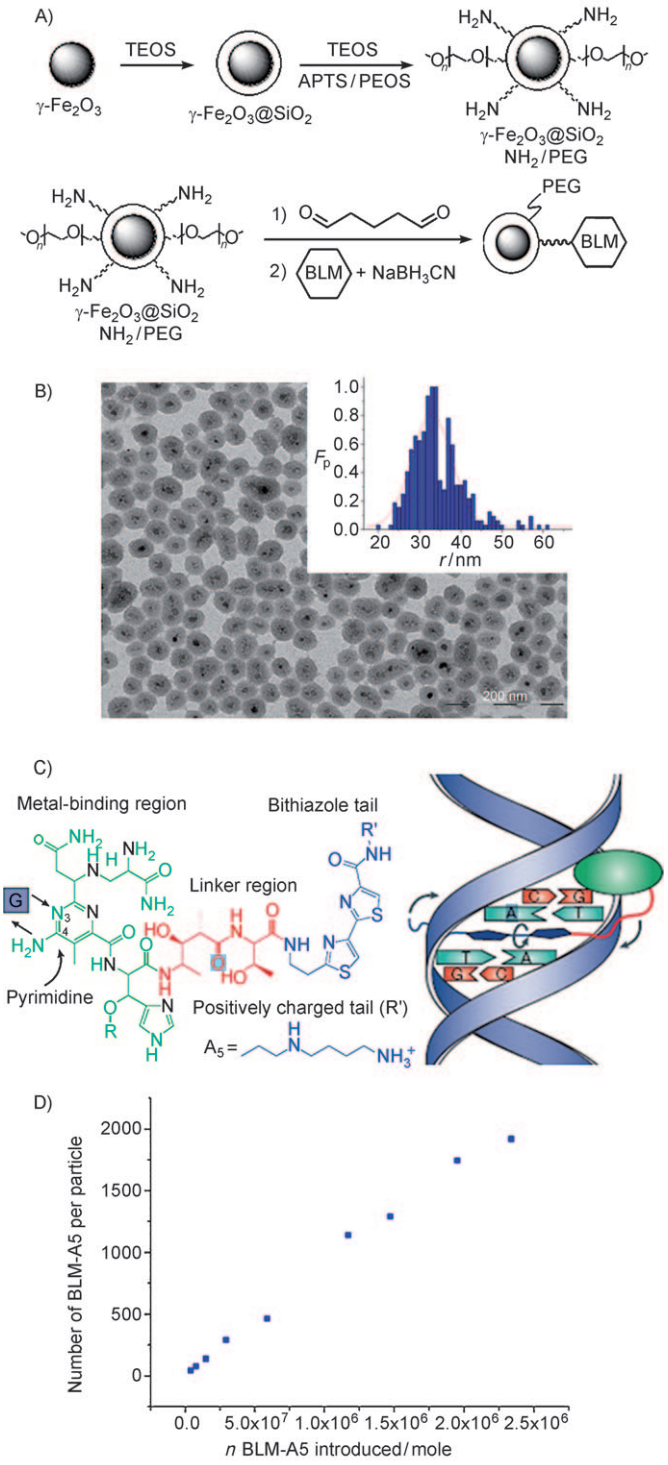

Figure 1. A) Nanoparticle synthesis and BLM anchoring. B) TEM image of CSMNs and their size distribution (inset). F_p = normalized particle frequency; r = physical diameter. C) BLM structure and DNA intercalation.[15] D) BLM-A5 per nanoparticle as a function of the amount of BLM-A5 introduced. TEOS = tetraethyl orthosilicate.

through the C-terminal BLM moiety using a glutaraldehyde linker. A wide range of BLM@CSMNs can be prepared with various amounts of BLM-A5 grafted to the surface. The grafting efficiency is about 17%, and by varying the quantity of introduced BLM-A5, CSMNs containing between 100 and 2000 BLM-A5 units per CSMN were obtained (Figure 1D). CSMNs with the highest BLM-A5 surface density were used for all the biochemical and cellular experiments. These BLM@CSMNs can be dispersed in 100 mM MOPS buffer at pH 7.4 to produce a dispersion that stays stable over months, with a mean hydrodynamic particle diameter around 50 nm and a zeta potential of +11 mV.

The cleavage ability of BLM-A5 before and after anchoring was studied on supercoiled pUC19 DNA. After Fe^{II} activation of the BLM-A5, the ability of Fe^{II}-BLM and Fe^{II}-BLM@CSMNs to induce plasmid DNA relaxation was studied using agarose gel electrophoresis. Cleavage of DNA by Fe^{II}-BLM@CSMNs occurred from 2 μM (Figure 2A,

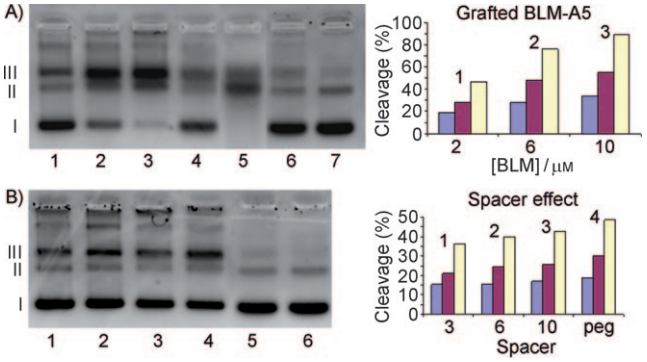

Figure 2. Agarose gel electrophoresis (SYBR green) and percentages of DNA cleavage (histograms). A) Comparison of strand scission of plasmid DNA pUC19 by Fe^{II}-BLM@CSMNs (lanes 1–3) or Fe^{II}-BLM-A5 (lanes 4 and 5). Equimolar amounts of Fe^{II} and BLM-A5 (grafted or free) were introduced in each lane. Lane 1: 2 μM; lane 2: 6 μM; lane 3: 10 μM; lane 4: 0.5 μM; lane 5: 2 μM. Lane 6: control incubation of plasmid DNA pUC19 with 10 μM Fe^{II}. Lane 7: plasmid DNA pUC19. B) Comparison of strand scission of plasmid DNA Puc19 by Fe^{II}-BLM@CSMNs synthesized with different spacer lengths (lanes 1–4). Two micromoles of Fe^{II} and BLM@CSMNs were introduced in each lane. Lane 1: spacer C3; lane 2: spacer C6; lane 3: spacer C10; lane 4: spacer PEG_{1500}; lane 5: control incubation of plasmid DNA pUC19 with 2 μM Fe^{II}; lane 6: plasmid DNA pUC19. Histograms: blue bars, one DNA cleavage; red bars, two DNA cleavages; yellow bars, total DNA cleavage.

lane 1), whereas at 10 μM around 90% of the plasmid was cleaved (Figure 2A, lane 3). In comparison, free Fe^{II}-BLM-A5 cleaved around 50% of the plasmid at 0.5 μM (Figure 2A, lane 4), whereas around 90% of plasmid cleavage was observed at 2 μM (Figure 2A, lane 5). These results demonstrate that grafted BLM-A5 kept its ability to cleave DNA once grafted onto CSMNs. Moreover, Fe^{II}-BLM@CSMNs are active in the same range of concentrations as free BLM-A5. Interestingly, we found that Fe^{II}-BLM@CSMNs induced predominantly double-strand DNA scissions (form III). The cause may be that, on nanoparticles, several BLM-A5 molecules are close together, thus favoring two DNA cleavage sites at the same time. The small efficiency decrease of grafted BLM compared with the free compound can be explained by a decrease of BLM-A5 accessibility to DNA. Indeed, a moderate improvement of the scission efficiency

can be obtained by increasing the amino spacer length (Figure 2B). For the same concentration of grafted BLM-A5, use of a PEG spacer led to a small increase (ca. 10%) of cleavage efficiency in comparison with the C3 spacer generally used.

The ability of Fe^{II}-BLM@CSMNs to induce telomeric (TTAGGG TTAGGG TTAGGG TTAGGG) DNA cleavage was evaluated. After 5′ labeling with ^{32}P, the telomeric dsDNA was incubated with Fe^{II}-BLM-A5 or Fe^{II}-BLM@CSMNs and the reaction was analyzed by denaturing gel electrophoresis. Sites of cleavage were identified using Maxam–Gilbert sequencing as a control. Identical sequence-selective cleavage was observed for Fe^{II}-BLM-A5 and Fe^{II}-BLM@CSMNs. Main cleavages were observed for GT sites whereas GG sites were weakly cleaved, as reported in the literature (see Figure S1 in the Supporting Information).[22–24] The preservation of cleavage efficiency and selectivity indicates that BLM-A5 grafted onto CSMNs allows efficient in vitro bithiazole intercalation and metal binding site orientation.

Cellular studies were carried out using human fibrosarcoma HT1080 as a cellular model and Cu^{II}-BLM-A5. It is well known that BLM-A5 activation requires iron–BLM chelation,[15] but *in cellulo* transmetalation is required to improve mediated BLM-A5 DNA cleavage.[25] Intracellular localization of Cu^{II}-BLM@CSMNs and CSMNs was first characterized by confocal microscopy using fluorescent CSMNs (rhodamine dye). Both CSMNs and Cu^{II}-BLM@CSMNs showed good intracellular uptake. Statistical analysis of internalized nanoparticles was performed by counting fluorescent cells. For the same amount of incubated particles (60 μg) and incubation time (48 h), 83% of cells incorporated CSMNs whereas 97% of cells incorporated Cu^{II}-BLM@CSMNs. Moreover, CSMNs and Cu^{II}-BLM@CSMNs were observed close to the nucleus (Figure 3A and B). Any particles were localized in the cytoplasmic membrane, thus indicating that all the internalized nanoparticles are confined close to the nucleus. Interestingly, Cu^{II}-BLM@CSMNs seem to have a higher interaction with the nuclear membrane than CSMNs. Figure 3B and C are images of the same cell at different depths. One can clearly see co-localization of Cu^{II}-BLM@CSMNs and the nucleus, a proof of nuclear membrane translocation. Often, a chromatin shift was observed (Figure 3D, left), which can be an indication of nuclear membrane deformation, as 3D rendering of the image seems to confirm (Figure 3D, right).

Secondly, the mechanism for Cu^{II}-BLM@CSMN and CSMN internalization and localization was clarified by TEM. Kinetic studies of nanoparticle uptake were conducted to follow the migration of nanoparticles in cells. After 30 min of incubation, Cu^{II}-BLM@CSMNs were observed mainly near the cytoplasmic membrane. Individual nanoparticles were observed in the cytosol membrane (Figure 4A and B). This observation could be the result of a fast diffusive internalization pathway, a mechanism reported only for small, charged nanoparticles.[10,26] At the same incubation time, Cu^{II}-BLM@CSMNs embedded in vesicles were also observed, thus revealing a more classical endocytosis internalization pathway (Figure 4C and D). For longer incubation times,

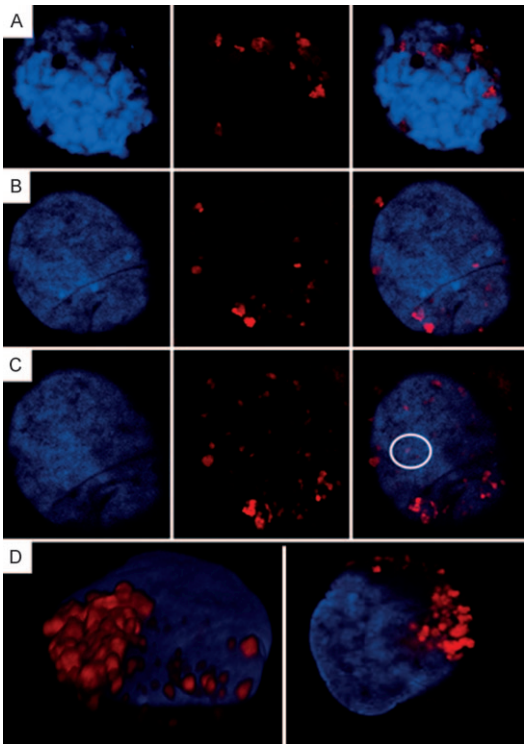

Figure 3. Co-localization of rhodamine-fluorescent CSMNs or Cu^{II}-BLM@CSMNs and nucleus, which was stained with 4′,6-diamidino-2-phenylindole (DAPI). After 48 h of incubation of HT1080 cells with CSMNs (A) or Cu^{II}-BLM@CSMNs (B–D), the cells were fixed and processed using dual-label immunofluorescence confocal microscopy. A–C) The images are each composed of two single-color images at a single *z*-slice (left: nucleus, middle: nanoparticles) and one merged color image at a single *z*-slice (right). B,C) Images of the same cell at different depths. D) 3D rendering image (left) and a merged color image at a single *z*-slice (right). The white circle in (C) identifies nanoparticles inside the nucleus. Other nanoparticles seem to be localized close to the nucleus, inside nucleus walls.

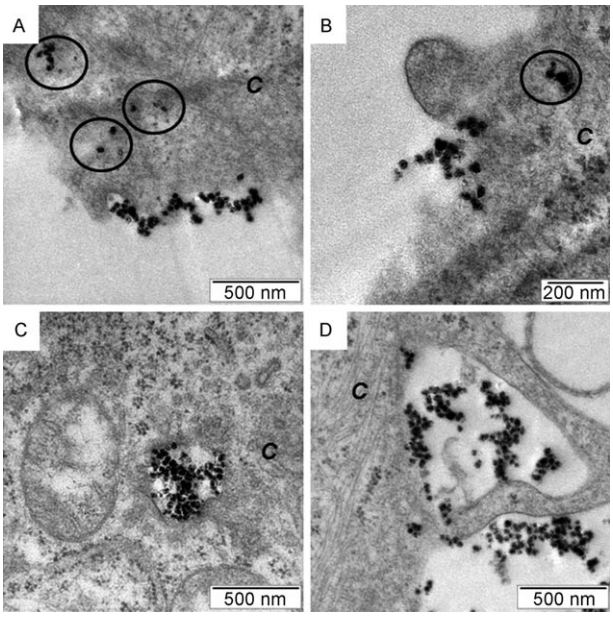

Figure 4. Representative TEM images of an HT1080 cell treated with Cu^{II}-BLM@CSMNs after 30 min of incubation. C: cytoplasm. Black circles indicate diffusive nanoparticles.

Cu^{II}-BLM@CSMNs were always observed in endosomes, which suggests that the individual nanoparticles observed at shorter times were later incorporated into vesicles. After 24 h of incubation, Cu^{II}-BLM@CSMNs appeared as agglomerates inside 400 nm endosomes (Figure 5 A). Endosome sizes

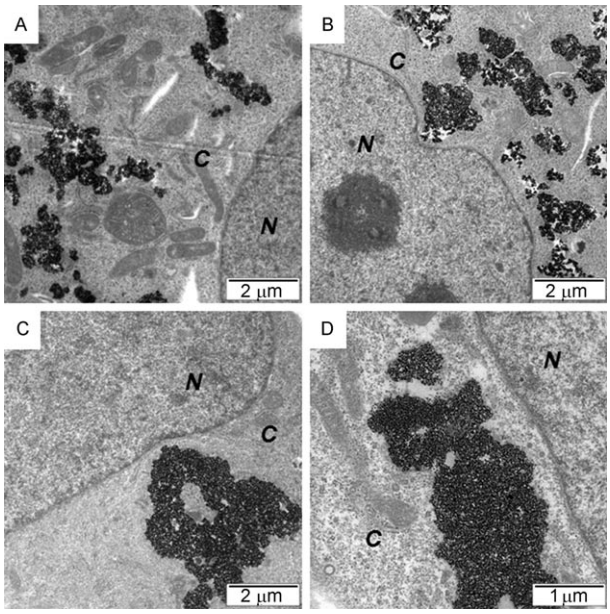

Figure 5. Representative TEM images of an HT1080 cell treated with Cu^{II}-BLM@CSMNs after 24 (A), 48 (B), and 96 h (C, D) of incubation. C: cytoplasm, N: nucleus.

increased with time while approaching the nuclear membrane and, according to confocal microscopy, deformation of the nuclear membrane by large endosomes was observed at 48 h (Figure 5 B) and 96 h (Figure 5 C and D). The same internalization mechanisms and migration kinetics were observed for CSMNs (see Figures S2 and S3 in the Supporting Information).

Moreover, Cu^{II}-BLM@CSMNs and CSMNs were clearly observed in the nucleus (Figure 6 A,B and Figure S4 in the Supporting Information), thus proving that this nanometric vector is able to cross the nuclear membrane. Therefore, this nanoplatform is able to convey BLM near to its biological target, DNA, without mediation of nuclear penetration molecules such as peptides.[27] As a consequence of the nuclear internalization of the BLM, apoptotic nuclei were observed (Figure 6 C) for cells incubated with Cu^{II}-BLM@CSMNs, but this effect was not observed for CSMNs. In addition, Cu^{II}-BLM@CSMNs and CSMNs were observed in mitochondria, which are potential therapeutic targets when they are implicated in cell growth. Mitochondria with incorporated Cu^{II}-BLM@CSMNs showed structural damage, such as dilution of the matrix caused by cristolysis mechanisms (Figure 6 D and E).

Finally, in vitro cytotoxicity of CSMNs and Cu^{II}-BLM@CSMNs was evaluated by cell growth and clone efficiency measurements on HT1080 cells. Cell growth measurements (Figure 7) indicated that Cu^{II}-BLM@CSMNs

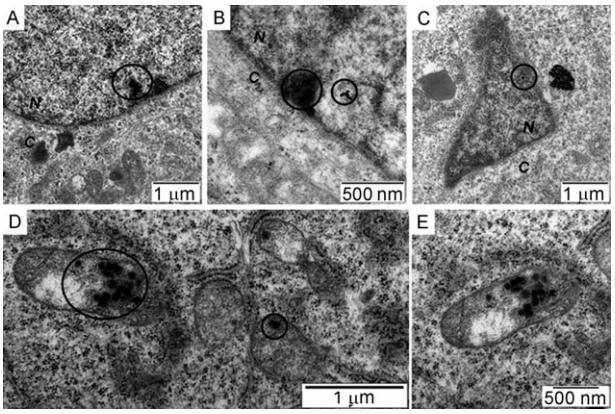

Figure 6. Representative TEM images of an HT1080 cell treated with Cu^{II}-BLM@CSMNs after 30 min of incubation. C: cytoplasm, N: nucleus. Black circles indicate nanoparticles in the nucleus (A–C) and in mitochondria (D, E).

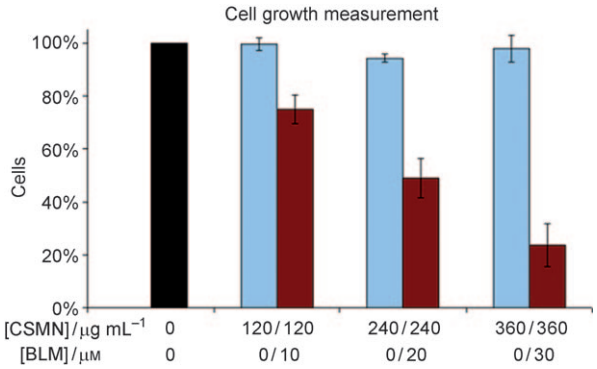

Figure 7. Percentage of living cells after 48 h of incubation at 37 °C with CSMNs (red bars) or Cu^{II}-BLM@CSMNs (blue bars). The [CSMN] scale indicates the mass concentration of nanoparticles for both experiments. The [BLM] scale indicates the resulting BLM-A5 molar concentration for Cu^{II}-BLM@CSMNs. The control is untreated cells incubated under the same conditions (black bar). Each data point represents the mean value of two sample duplicates.

induced up to a 90 % decrease in the number of living cells in comparison with untreated reference cells. Interestingly, dead cells only made up 2 % of all cells counted, thus suggesting a growth arrest. In contrast, CSMNs showed almost no cytotoxic effect for the same nanoparticle concentrations.

To understand the results obtained by cell growth measurements, a clonogenic efficiency measurement was performed. This assay allows characterization of the capacity of cells to produce clones and was performed on cells incubated with CSMNs and Cu^{II}-BLM@CSMNs. Selected viable cells with incorporated Cu^{II}-BLM@CSMNs (20 μM of BLM) produced small numbers of cloned cells (10 % clonogenic efficiency), whereas cells with incorporated CSMNs were able to reproduce themselves normally (90 % clonogenic efficiency). These results indicate that the strong decrease in the number of living cells can be mainly explained by a growth arrest, caused by interactions between Cu^{II}-BLM@CSMNs and the nucleus and mitochondria.

We have succeeded in designing a biocompatible hybrid therapeutic nanoplatform able to convey BLM while maintaining its cytotoxic activity. Moreover, nanoparticles allow interactions between BLM and both nucleus and mitochondria, thus resulting in an inhibition of cell growth. In light of these results, CSMNs have great potential for the delivery of BLM-A5 to tumors while improving its biodistribution.

Received: June 1, 2010
Published online: October 7, 2010

Keywords: bleomycin · cytoxicity · drug delivery · nanoparticles · theranostics

[1] a) R. K. Jain, *Annu. Rev. Biomed. Eng.* **1999**, *1*, 241 – 263; b) E. Helm, *Eukaryon* **2007**, *3*, 55 – 62; c) R. K. Jain, *J. Controlled Release* **1998**, *53*, 49 – 67.

[2] a) K. Strebhardt, A. Ullrich, *Nat. Rev.* **2008**, *8*, 473 – 480; b) E. Gullotti, Y. Yeo, *J. Mol. Pharm.* **2009**, *6*, 1041 – 1051; c) A. Vincent, S. Babu, E. Heckert, J. Dowding, S. M. Hirst, T. M. Inerbaev, W. T. Self, C. M. Reilly, A. E. Masunov, T. S. Rahman, S. Seal, *ACS Nano* **2009**, *3*, 1203 – 1211.

[3] a) M. E. Davis, Z. Chen, D. M. Shin, *Nat. Rev.* **2008**, *7*, 771 – 782; b) R. Duncan, *Nat. Rev.* **2006**, 688 – 701; c) M. Ferrari, *Nat. Rev.* **2005**, *5*, 161 – 171; d) D. A. Lavan, T. McGuire, R. Langer, *Nat. Biotechnol.* **2003**, *21*, 1184 – 1191; e) K. Riehemann, S. W. Schneider, T. A. Luger, B. Godin, M. Ferrari, H. Fuchs, *Angew. Chem.* **2009**, *121*, 886 – 913; *Angew. Chem. Int. Ed.* **2009**, *48*, 872 – 897.

[4] a) J. Kim, Y. Piao, T. Hyeon, *Chem. Soc. Rev.* **2009**, *38*, 372 – 390; b) H.-T. Song, J.-S. Choi, Y.-M. Huh, S. Kim, Y.-W Jun, J.-S. Suh, J. C. Song, *J. Am. Chem. Soc.* **2005**, *127*, 9992 – 9993; c) H. Lee, M. K. Yu, S. Park, S. Moon, J. J. Min, Y. Y. Jeong, H.-W. Kang, S. Jon, *J. Am. Chem. Soc.* **2007**, *129*, 12739 – 12745; d) E. Taboada, E. Rodriguez, A. Roig, J. Oro, A. Roch, R. N. Muller, *Langmuir* **2007**, *23*, 4583 – 4588; e) C. Sun, J. S. H. Lee, M. Zhang, *Adv. Drug Delivery Rev.* **2008**, *60*, 1252 – 1265; f) M.-Ch. Daniel, D. Astruc, *Chem. Rev.* **2004**, *104*, 2933 – 2946.

[5] a) J.-P. Fortin, C. Wilhelm, J. Servais, C. Menager, J.-C. Bacri, F. Gazeau, *J. Am. Chem. Soc.* **2007**, *129*, 2628 – 2635; b) M. Lévy, C. Wilhelm, J.-M. Siaugue, O. Horner, J.-C. Bacri, F. Gazeau, *J. Phys. Condens. Matter* **2008**, *20*, 1 – 5; c) B. Thiesen, A. Jordan, *Int. J. Hyperthermia* **2008**, *24*, 467 – 474.

[6] a) J. Kim, S. Park, J. E. Lee, S. M. Jin, J. H. Lee, I. S. Lee, I. Yang, J.-S. Kim, S. K. Kim, M.-H. Cho, T. Hyeon, *Angew. Chem.* **2006**, *118*, 7918 – 7922; *Angew. Chem. Int. Ed.* **2006**, *45*, 7754 – 7758; b) Y. Sun, Z.-L. Chen, X.-X. Yang, P. Huang, X.-P. Zhou, X.-X. Du, *Nanotechnology* **2008**, *20*, 1 – 8.

[7] a) H. Maeda , J. Wu, T. Sawaa, Y. Matsumura, K. Hori, *J. Controlled Release* **2000**, 65, 271 – 284; b) W. L. Monsky, D. Fukumura, T. Gohongi, M. Ancukiewcz, H. A. Weich, V. P. Torchilin, F. Yuan, R. K. Jain, *Cancer Res.* **1999**, *59*, 4129 – 4135.

[8] a) J. D. Byrne, T. Betancourt, L. Brannon-Peppas, *Adv. Drug Delivery Rev.* **2008**, *60*, 1615 – 1626; b) D. Schrama, R. A. Reisfeld, J. C. Becker, *Nat. Rev.* **2006**, *5*, 147 – 159.

[9] a) M. Links, R. Brown, *Expert Rev. Mol. Med.* **1999**, *1*, 1 – 21; b) V. Ling, *Cancer Chemother. Pharmacol.* **1997**, *40*, S3 – S8.

[10] a) A. Verma, F. Stellacci, *Small* **2010**, *6*, 12 – 21; b) H. Hillaireau, P. Couvreur, *Cell. Mol. Life Sci.* **2009**, *66*, 2873 – 2896; c) J. E. Fuller, G. T. Zugates, L. S. Ferreira, S. O. Hooisweng, N. N. Nguyen, U. B. Wiesner, R. S. Langer, *Biomaterials* **2008**, *29*, 1526 – 1532.

[11] S. M. Moghimi, A. C. Hunter, J. C. Murray, *Pharmacol. Rev.* **2001**, *53*, 283 – 318.

[12] a) S. C. McBain, H. P. Yiu, J. Dobson, *Int. J. Nanomed.* **2008**, *3*, 169 – 180; b) Ref. [4c]; c) M. K. Yu, Y. Y. Jeong, J. Park, S. Park, J. W. Kim, J. J. Min, K. Kim, S. Jon, *Angew. Chem.* **2008**, *120*, 5442 – 5445; *Angew. Chem. Int. Ed.* **2008**, *47*, 5362 – 5365; d) T. K. Jain, M. K. Reddy, M. A. Morales, D. L. Leslie-Pelecky, V. Labhasetwar, *J. Mol. Pharm.* **2008**, *2*, 194 – 205; e) J. Kim, H. S. Kim, N. Lee, T. Kim, H. Kim, T. Yu, I. C. Song, W. K. Moon, T. Hyeon, *Angew. Chem.* **2008**, *120*, 8566 – 8569; *Angew. Chem. Int. Ed.* **2008**, *47*, 8438 – 8441; f) T.-J. Yoon, J. S. Kim, B. G. Kim, K. N. Yu, M.-H. Cho, J. K. Lee, *Angew. Chem.* **2005**, *117*, 1092 – 1095; *Angew. Chem. Int. Ed.* **2005**, *44*, 1068 – 1071; g) T.-J. Yoon, K. N. Yu, E. Kim, J. S. Kim, B. G. Kim, S.-H. Yun, B.-H. Sohn, M.-H. Cho, J.-K. Lee, S. B. Park, *Small* **2006**, *2*, 209 – 215; h) M. Liong, J. Lu, M. Kovochich, T. Xia, S. G. Ruehm, A. E. Nel, F. Tamanoi, J. I. Z. Liong, *ACS Nano* **2008**, *2*, 889 – 896.

[13] a) D. E. Owens III, N. A. Peppas, *Int. J. Pharm.* **2006**, *307*, 93 – 102; b) L. E. van Vlerken, T. K. Vyas, M. M. Amiji, *Pharm. Res.* **2007**, *24*, 1405 – 1414; c) H. Otsuka, Y. Nagasaki, K. Kataoka, *Adv. Drug Delivery Rev.* **2003**, *55*, 403 – 419.

[14] a) V. Maurice, T. Georgelin, J.-M. Siaugue, V. Cabuil, *J. Magn. Magn. Mater.* **2009**, *10*, 1408 – 1413; b) T. Georgelin, V. Maurice, B. Malizieux, J.-M. Siaugue, V. Cabuil, *J. Nanopart. Res.* **2010**, *12*, 675 – 680.

[15] J. Chen, J. Stubbe, *Nat. Rev.* **2005**, 5, 102 – 112.

[16] A. T. Abraham, X. Zhou, S. M. Hecht, *J. Am. Chem. Soc.* **2001**, *123*, 5167 – 5175.

[17] D. Guowei, K. Adriane, X. Chen, C. Jie, L. Yinfeng, *Int. J. Pharm.* **2007**, *328*, 78 – 85.

[18] R. Massart, J.-C. Bacri, R. Perzynski, D. Salin, *J. Magn. Magn. Mater.* **1986**, *62*, 36 – 46.

[19] N. Fauconnier, J. N. Pons, J. Roger, A. Bee, *J. Colloid Interface Sci.* **1997**, *194*, 427 – 433.

[20] a) A. van Blaaderen, A. Vrij, *Langmuir* **1992**, *8*, 2921 – 2931; b) D. Ma, A. J. Kell, S. Tan, Z. J. Jakubek, B. Simard, *J. Phys. Chem. C* **2009**, *113*, 15974 – 15981.

[21] F. d'Orlyé, A. Varenne, T. Georgelin, J.-M. Siaugue, B. Teste, S. Descroix, P. Gareil, *Electrophoresis* **2009**, *30*, 2572 – 2582.

[22] D. L. Boger, H. Cai, *Angew. Chem.* **1999**, *111*, 470 – 500; *Angew. Chem. Int. Ed.* **1999**, *38*, 448 – 476.

[23] S. M. Hecht, *Nat. Prod.* **2000**, *63*, 158 – 168.

[24] A. D. D'Andrea, W. A. Haseltine, *Proc. Natl. Acad. Sci. USA* **1978**, *75*, 3608 – 3612.

[25] J. H. Freedman, S. B. Horwitz, J. Peisach, *Biochemistry* **1982**, *21*, 2203 – 2210.

[26] M. Geiser, B. Rothen-Rutishauser, *Environ. Health Perspect.* **2005**, *113*, 1555 – 1560.

[27] A. G. Tkachenko, H. Xie, D. Coleman, W. Glomm, J. Ryan, M. F. Anderson, S. Franzen, D. L. Feldheim, *J. Am. Chem. Soc.* **2003**, *125*, 4700 – 4701.

